Carbohydrate Polymers 291 (2022) 119560

Contents lists available at ScienceDirect

Carbohydrate Polymers

journal homepage: www.elsevier.com/locate/carbpol

Self-assembly of ferria – nanocellulose composite fibres

T.C. Breijaert [a], G. Daniel [b], D. Hedlund [c], P. Svedlindh [c], V.G. Kessler [a], H. Granberg [d], K. Håkansson [d], G.A. Seisenbaeva [a,*]

[a] Department of Molecular Sciences, Biocentrum, Swedish University of Agricultural Sciences, Almas Allé 5, SE-756 51 Uppsala, Sweden
[b] Department of Forest Biomaterials and Technology, Wood Science, Swedish University of Agricultural Sciences, Vallvägen 9C-D, 756 51 Uppsala, Sweden
[c] Department of Materials Science and Engineering, Uppsala University, Box 35, 751 03 Uppsala, Sweden
[d] Department of Material and Surface Design, Smart Materials, Research Institutes of Sweden (RISE), Drottning Kristinas väg 61, 114 28 Stockholm, Sweden

ARTICLE INFO

Keywords:
Nanocellulose
Magnetite
Magnetic composites
Hybrid materials
Photo-induced drug delivery

ABSTRACT

An environmentally benign synthesis of a magnetically responsive carboxymethylated cellulose nanofibril-based material is reported. Applied experimental conditions lead to the in-situ formation of magnetite nanoparticles with primary particle sizes of 2.0–4.0 nm or secondary particles of 3.6–16.4 nm depending on whether nucleation occurred between individual carboxymethylated cellulose nanofibrils, or on exposed fibril surfaces. The increase in magnetite particle size on the cellulose fibril surfaces was attributed to Ostwald ripening, while the small particles formed within the carboxymethyl cellulose aggregates were presumably due to steric interactions. The magnetite nanoparticles were capable of coordinating to carboxymethylated cellulose nanofibrils to form large "fibre-like" assemblies. The confinement of small particles within aggregates of reductive cellulose molecules was most likely responsible for excellent conservation of magnetic characteristics on storage of this material. The possibility for using the material in drug delivery applications with release rate controlled by daylight illumination is presented.

1. Introduction

The UN 2030 agenda for sustainable development, highlights key areas where the development of sustainably produced materials is expected to play a crucial role (*Transforming Our World: The 2030 Agenda for Sustainable Development | Department of Economic and Social Affairs*, n. d.). It emphasizes the need for development of innovative solid materials for key applications, such as smart packaging, advanced adsorbents, wound healing and tissue engineering scaffolds using environmentally sustainable raw materials. Major focus today is therefore set on natural bio-based polymers.

Cellulose is the most abundant renewable polymer on the planet accounting for multiple teratons of annual biomass production (Klemm et al., 2005). Cellulose is found in all plant forms where it often forms the major constituent (e.g. cotton, wood). Historically and currently, these plant derived forms of cellulose have been used for everyday applications in the form of fabrics, pulp and paper and wood constructions (Hon, 1994).

Potentially industrially important forms of cellulose can also be derived from higher order structures, which have been physically and/or chemically treated to produce nano-sized cellulose nanofibrils (CNFs, nanocellulose) or cellulose nanocrystals (CNCs). The latter can be used in polymer matrices (Favier et al., 1995; Grunert & Winter, 2002; Oun & Rhim, 2017) as actuators (Hartings et al., 2018; Kim et al., 2006) and transistors (Lim et al., 2009), etc. (Arantes et al., 2017; Hu et al., 2009; Khalilzadeh et al., 2020; Wu et al., 2018). Due to its bio-availability, biocompatibility, and chemical functionality, cellulose is an attractive material for use in environmentally benign applications (Klemm et al., 2005).

One of the major challenges in the development and adaptation of cellulose-based materials is its relative inertness. In order to expand its usage beyond that of simple fibres or crystals, cellulose must be chemically modified to not only increase its solubility but also to diversify and increase the range of possible applications. The development of carboxymethyl cellulose (CMC) for example has led to its use in food as well as more technical applications such as protein purification (Hao et al., 2021; He et al., 2021) and coatings (Dimic-Misic et al., 2013; Souza et al., 2019). Properties of nanocellulose-derived materials are related to size, morphology and surface chemistry of the particles. The nanoparticles can be cellulose nanocrystals (CNC), cellulose nanofibres (CNF)

* Corresponding author.
E-mail address: gulaim.seisenbaeva@slu.se (G.A. Seisenbaeva).

https://doi.org/10.1016/j.carbpol.2022.119560
Received 18 February 2022; Received in revised form 12 April 2022; Accepted 28 April 2022
Available online 3 May 2022

or bacterial cellulose fibres (BCF) (Sacui et al., 2014).

A significant number of studies to date involving the use of natural biopolymers for advanced technical solutions have focussed on the incorporation of responsive metal oxide materials into, or onto a biopolymer matrix. By including the spinel-type iron oxides such as magnetite or iron(II)-deficient maghemite into biopolymer matrices, composite materials may be obtained with favourable magnetic and catalytic properties. These characteristics may be exploited in the development of materials suitable for applications as Magnetic Resonance Image contrasting agents (Abbasi Pour et al., 2017; Biliuta et al., 2017), antibacterial agents (Biliuta et al., 2017), in magneto-optical applications (Chen et al., 2020; Li et al., 2013), protein adsorption membranes (Wu et al., 2018), metal ion removal (Yu et al., 2012, 2014), electrochemical sensors (Khalilzadeh et al., 2020) and for medical applications (Abbasi Pour et al., 2017; Chaabane et al., 2020).

With magnetically responsive cellulose-iron oxide composite materials, work has focussed on the production of materials either by incorporating pre-synthesized iron oxide particles into a fibril-matrix or via the in-situ growth of particles onto pre-formed biopolymer fibrils/fibres surfaces. Numerous techniques have been developed for production of nano-ferria in a broad range of sizes and morphologies. They include solvothermal synthesis starting from organic precursors or iron carbonyl, resulting in small uniform well-crystallized particles that are often rendered hydrophobic by the conditions of synthesis. An alternative approach is based on co-precipitation in aqueous media. Its drawback lies, however, in relatively appreciable solubility of ferria in polar aqueous media that can result in considerable size variation because of the Ostwald ripening (Thanh, 2012). The challenge in use of pre-formed particles lies in the difficulty of their uniform distribution. With the synthesis of composites, attention has generally been towards in-situ particle growth on a matrix. For efficient distribution of the inorganic content, the matrix should be activated via surface oxidation or esterification. The reactivity of cellulose resembles in this case that of graphene oxide with oxidized surface groups, for example by carboxylation (Dimic-Misic et al., 2019). To our knowledge, no reports have so far been made on cellulose based nanocomposite materials where magnetic iron oxides and nanocellulose self-assemble into large fibre-like structures. In earlier studies, focus was on the in-situ formation of magnetite nanoparticles on relatively large, unmodified, cellulose nanofibres, resulting in the formation of magnetite particle decorated nanofibres with metal oxide particles greater than 10 nm (Galland et al., 2013).

Our hypothesis was that producing magnetic iron oxide in-situ in the presence of highly functionalized nano cellulose would result in a dense self-assembled material with:

1) Potentially interesting morphologies;
2) Stable magnetic characteristics (through protection of magnetic particles within a dense composite through encapsulation in a reductive matrix); *and*
3) Capacity for visible light controlled release of adsorbed pharmaceuticals, exploiting photo magnetic properties of the obtained composite material.

2. Materials and methods

2.1. Materials

Carboxymethylated nanocellulose fibrils (C-CNF, derived from wood, Degree of Substitution (DS) of cellulose surface hydroxyl groups 0.098) was prepared at RISE Bioeconomy and Health according to the method of Wågberg et al. (2008) as a hydrogel with solid concentration 2.26% by weight. DS is the (average) number of substituent groups attached per base unit (in the case of condensation polymers) or per monomeric unit (in the case of addition polymers). The term has been mainly used in cellulose chemistry. The DS value indicates that approximately 10% of all hydroxyl groups have been carboxymethylated (Wågberg et al., 2008). After carboxymethylation of a softwood sulphite dissolving pulp (Domsjö Dissolving Plus), the cellulose material was passed through a homogeniser (Microfluidizer M-110EH, Microfluidics Corp., USA) at 1700 bar with two serial chambers of 200- and 100 μm, respectively. The carboxylate content of the nanocellulose was determined via conductometric titration. The C-CNF applied here differs in its characteristics from TEMPO oxidized nano cellulose in that it has a combination of both carboxyl- and carboxymethyl surface functional groups, while TEMPO-CNF has aldehyde and carboxyl groups (Aaen et al., 2019). In addition, the crystal structure is a slightly different between the two grades. Furthermore, the mechanical treatment to delaminate the pulp fibres into fibrils induces variations and commonly the C-CNF has more residual fibre fragments, unless extra cleaning and separation steps are performed.

Iron(II) sulphate heptahydrate (pro analysis), anhydrous iron(III) chloride, and ammonia (25% based on NH_3) were obtained from Sigma-Aldrich, Sweden AB. All chemicals were used without further purification. Water was purified using a Millipore system and purged with nitrogen for several hours prior to use. Ammonia solution was prepared using nitrogen purged water and stored under nitrogen.

2.2. Characterization

Samples were characterized using a Bruker Dimension FastScan Atomic Force Microscope (AFM) with a Nanoscope V controller in ScanAsyst mode using a Fastscan-B AFM probe (silicon tip, f_0: 400 kHz, k:4 N/m, tip radius: 5 nm nominally) and a scan rate of 1-3 Hz. Samples were prepared on freshly exfoliated mica. Data was processed using Gwyddion 2.56 with align rows-median to remove skipping lines.

Scanning Electron Microscopy (SEM) observations were conducted using a Hitachi FlexSEM 1000 at an acceleration voltage of 5 kV, spot size 20, and 5 mm working distance. Samples were prepared on Cu foil from aqueous suspensions.

For Transmission Electron Microscopy (TEM), ethanol exchanged oxides were deposited on holey carbon grids (Pelco® 50 mesh grids: Pitch 508 μm; hole width 425 μm; bar width 83 μm; transmission 70%) and observed using a Philips CM/12 microscope (Thermo Fisher Inc.) fitted with LaB6 and operated at 80 or 100 kV. Oxide treated C-CNFs were also embedded in LR White resin (London Resin Co., Basingstoke, UK) following dehydration in ethanol (20–100%, 20% steps, 5 min each). Ultrathin sections (70–100 nm thickness) were cut using a Reichert Ultracut E ultramicrotome and collected on copper grids. Negative TEM films were scanned using an Epson Perfection Pro 750 film scanner. Sections were observed unstained or after post staining with 2% w/v aq. uranyl acetate (10 min) at 80–100 kV.

Powder X-ray Diffraction (PXRD) data was obtained using lyophilized samples on a Bruker APEX-II diffractometer equipped with an AXS Smart APEX CCD Area Detector and graphite-monochromated Mo-K_α (λ = 0.71073 Å) radiation source. Data was processed with the EVA-12 software package.

Fourier Transform Infrared (FTIR) analysis was done on a Perkin Elmer Spectrum 100 FT-IR Spectrometer using KBr pellets. Thermogravimetric Analysis (TGA) was done using a Perkin Elmer Pyris 1 TGA at a heating rate of 5 °C/min.

Magnetic measurements were performed using a Lake Shore Cryotronics Series 7400 vibrating sample magnetometer (VSM). Measurements were performed at 300 K (26,85 °C) in the magnetic field range ±10 kOe with the magnetic moments normalized using the weight of iron oxide solid phase.

2.3. Synthesis

22.089 g of 2.26 wt% C-CNF (499 mg solid C-CNF) was transferred to a 250 mL round bottom flask equipped with a Teflon coated stirring bean and nitrogen inlet. C-CNF suspended in 200 mL nitrogen purged ultrapure water was added and vigorously stirred for 30 min. Then, 327

mg $FeCl_3$ (2.02 mmol) and 328.5 mg (1.18 mmol) $FeSO_4{\cdot}7H_2O$ was added, forming a 1.7:1 stoichiometry between Fe^{3+}/Fe^{2+} and concentration of 9.10 mM Fe^{3+}/5.33 mM Fe^{2+} respectively. The pH was adjusted to pH 5 (according to litmus), using 0.5 mM HCl and the suspension allowed to stir for 30 min at room temperature under a constant flow of bubbling nitrogen. Then, 1.5 M NH_4OH was added dropwise using a syringe until pH 9 (according to litmus). Stirring was stopped and the particles allowed to settle for 5 min, before decanting into 50 mL falcon tubes and washing 4× with N_2-purged ultrapure water and collection via centrifugation (10 min, 5000 RPM).

2.4. Adsorption experiments

An aliquot equating to ca. 15 mg composite material was removed and mixed with ca. 3 mg tetracycline, placed in an aluminium-wrapped falcon tube and diluted to a final volume of 40 mL. This was placed on an orbital shaker and allowed to shake for several days. Periodically, aliquots were taken and the composite collected via a strong magnet. The supernatant was measured using UV–VIS at 357 nm. Experiments were repeated in triplicate for reproducibility.

2.5. Desorption experiments

An aliquot equating to ca. 15 mg composite material was taken and mixed with ca. 3 mg tetracycline in a 50 mL pointed flask fitted with a stirring bar and diluted to 30 mL. The flask was heated overnight at 50 °C in a darkened fume hood with the setup wrapped in aluminium to avoid incident light. After stirring overnight, the product was cooled to room temperature and divided equally into two aluminium wrapped falcon tubes. The composite material was collected using a strong magnet, and the supernatant removed and diluted to 17 mL with 0.02 M citrate buffer (pH 6.0). One of the aluminium jackets was removed and both samples placed on an orbital shaker under a daylight lamp. Aliquots were periodically removed, the composite collected, and the tetracycline content in the supernatant determined via UV–VIS at 357 nm. Experiments were repeated in triplicate for reproducibility.

3. Results and discussion

3.1. Production of iron oxide in the presence of carboxymethylated nanocellulose fibrils

Magnetite is an easily produced magnetic metal oxide with an inverse spinel structured metal oxide consisting of iron(III) and iron(II) in a 1:2 stoichiometry which may be produced by co-precipitation in the presence of ammonia in the following reaction:

$$2Fe^{III}Cl_3 + Fe^{II}SO_4 + 8\,NH_4OH \rightarrow Fe_3O_4 + 6NH_4Cl + NH_4SO_4 + 4H_2O$$

Dissolution of Fe(II) and Fe(III) salts in the presence of C-CNFs followed by the slow addition of ammonia lead to the formation of a slight orange hued suspension, with the suspension darkening to a reddish-brown and then black as the pH increased. When the final pH was achieved, a black precipitate was present which slowly turned reddish-brown over time in the presence of ambient air due to the oxidation of Fe^{2+} to Fe^{3+}. Thermogravimetric analysis (SI Fig. S3) of the resulting sample showed a thermal decomposition temperature of 256–257 °C with a residual mass of 31.8 wt%.

3.2. Characterization of (bulk) composite material

3.2.1. XRD patterns of nanocomposite material

To determine which iron oxide phase is formed during the co-precipitation reaction of iron(II/III) in the presence of C-CNF, the powder X-ray pattern was measured and compared with certified

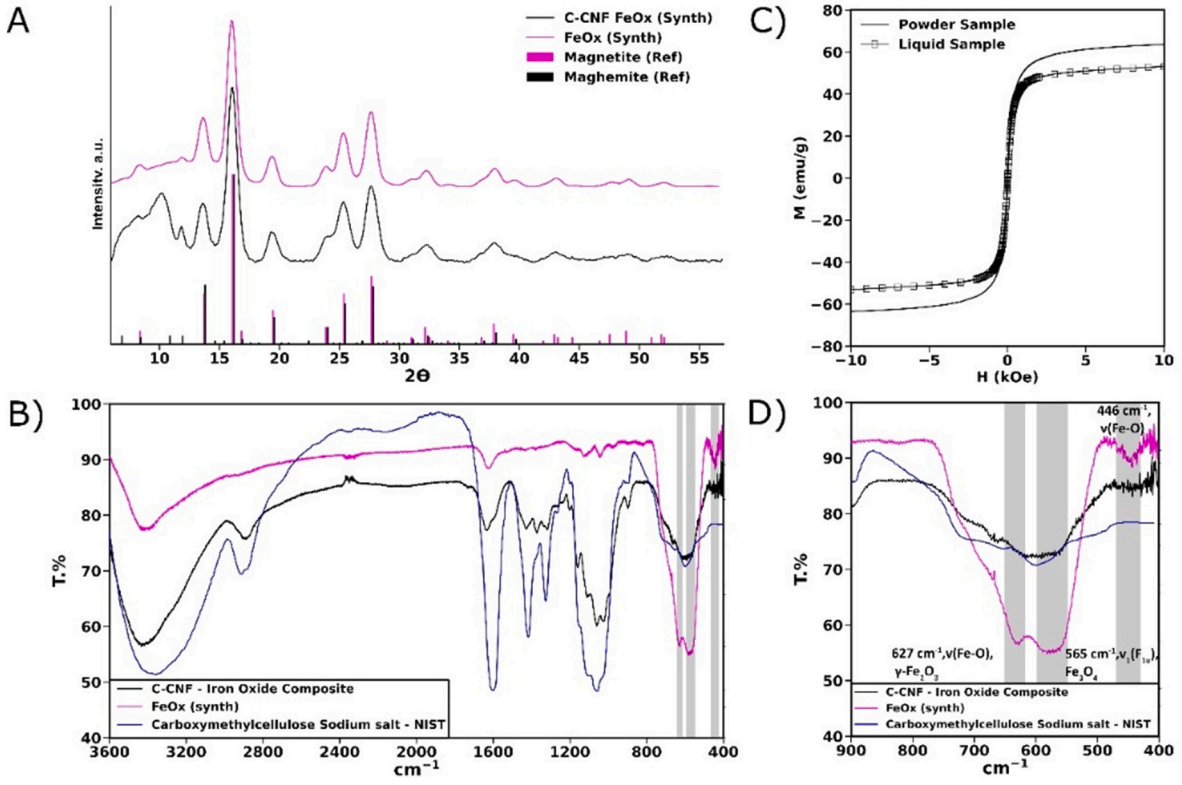

Fig. 1. A) PXRD pattern of a synthesized iron oxide – carboxymethylated cellulose nanofibril composite and iron oxide, measured using a Mo kα X-ray source. Maghemite (00-039-1346) and magnetite (00-019-0629) reference patterns overlaid. B) and D) Measured FTIR spectra of synthesized iron oxide–carboxymethylated cellulose nanofibril composite, magnetite and (sodium) carboxymethylated cellulose nanofibrils, NIST is the reference spectra. C) Magnetization vs magnetic field for powder and liquid samples.

patterns for both magnetite and the iron(II) deficient maghemite (Fig. 1A and SI Fig. S2). It was proven that the primary phase of the iron oxide formed in the presence of C-CNFs nanofibrils was magnetite, maghemite or a mixture of the two oxides. However, with the current setup it was impossible to differentiate between the two iron oxides. Scherrer analysis of the crystallite size was made applying the formula $\tau = K\lambda / (\beta \cdot \cos\Theta)$ and showed that the average size of freshly produced pure ferria under the applied conditions was 3.7 nm, while for the composite it was 3.4 nm. This shows that composite formation contributed to the preservation of smaller particles.

3.2.2. Fourier Transform Infrared spectroscopy (FTIR)

In an attempt to distinguish between the magnetite and maghemite iron oxides, the product was examined using FTIR. It should be noted however, that infrared spectroscopic results of magnetite/maghemite mixtures are not absolute due to a strong overlap of the most characteristics bands of iron oxides (Ellid et al., 2003). The iron oxide produced via in-situ precipitation of iron(III) chloride and iron(II) sulphate by ammonia is shown in Fig. 1B. The product obtained exhibits strong absorption bands at 627 and 576 cm^{-1}, with a minor adsorption band in the region of 446 cm^{-1}. Ishii et al. (1972) assigned the IR band at 565 cm^{-1} to the $\nu_1(F_{1u})$ vibration mode in magnetite, while a small shift to a higher wave number may be attributed to sub-stoichiometric magnetite (Ellid et al., 2003). The peak at 627 cm^{-1} can be assigned to the Fe—O vibration in the iron(II) deficient maghemite, which has formed due to oxidation (Klotz et al., 1999). The additional peaks at 1128, 1043, 975 cm^{-1} may be attributed to the presence of bound sulphate groups present in the sample (Musić et al., 2000). Finally, the peak observed at 1624 cm^{-1} and the broad peak at 3400 cm^{-1} can be attributed to moisture.

The produced iron oxide-C-CNF composite material exhibited similar absorption bands in the range 580–620 cm^{-1} with a smaller, less well-pronounced peak at 665 cm^{-1}, which is slightly shifted, compared to the synthesized magnetite sample. This may be attributed to the magnetite formed in the sample, being coordinated to carboxylate groups present in C-CNF with some maghemite having formed due to oxidation in air. Additional absorption bands appear at 2890, 1597, 1426, 1373, 1318, 1200, 1160, 1110, 1060, 1022, 897 cm^{-1} which are primarily attributed to the various absorption bands present within C-CNF.

3.2.3. Magnetic characterization

Fig. 1C shows the magnetization versus magnetic field for the powder and liquid samples. The measured magnetizations at an applied field of 10 kOe are 63 emu/g and 53 emu/g for the powder and liquid samples, respectively. Both values are somewhat smaller than expected for magnetite and maghemite, which may be explained by spin disorder and spin canting for surface spins in iron oxide nanoparticles. Moreover, as expected, the nanoparticles exhibit superparamagnetic behaviour at 300 K (26,85 °C) and hence zero remanence and coercivity. A plausible explanation for the minor drop in magnetization of the sample dispersed in ethanol is that partial oxidation has occurred with time, but only to rather low extent. The samples were stored for 10 months before measurements and thus revealed considerable stability against oxidation. Bulk magnetic properties are demonstrated in SI Fig. S4 and in a Supplementary video. The major volume of ferria was kept in the form of non-aggregated primary particles bound within the formed self-assembly fibres. This precludes both diffusion of oxygen and release of ions from the coordination-saturated surface of the particles. As a result – no apparent oxidation occurs on storage.

3.3. Morphological investigation of iron oxide composite materials

3.3.1. Atomic force microscopy

To examine the nanoscale structures formed when iron oxide is precipitated in the presence of C-CNFs, the sample was examined using AFM where it was apparent that the reaction is capable of producing a composite consisting of “fibre-like” structures (Fig. 2). Observations along the axis of these fibre-like structures showed random increases in surface height, likely attributed to the presence of iron oxide formed during the co-precipitation reaction.

The fibre-like structures observed had an average width of 18.55 ± 1.66 nm with lengths ranging from 70 nm to nearly a micrometer in longitudinal direction. However, the measured widths do not take tip convolution into account, which increases the observed widths compared to actual widths. By decreasing the measuring area to 200 × 200 nm (Fig. 2C, E), spherical to ellipsoidal particles were observed which appear surrounded by a C-CNF network.

The presence of multiple spherical to ellipsoidal particles across the longitudinal direction of the fibre-like structures (Fig. 2C, E) indicate that the iron oxide particles formed during the precipitation of iron(II) and iron(III) interact with the C-CNFs to form a composite material that self-assembled into fibre-like domains. This interesting property that should be exploited in future applications. However, it was impossible to determine from measured AFM data whether the particles were distributed on the actual surface of the network or within the C-CNF network itself without more detailed examination.

3.3.2. Electron microscopy

To supplement the AFM data, samples were prepared for SEM and TEM as described in the method section (Fig. 3). SEM confirmed that the fibre-like structures were not completely homogeneous showing aggregates along the surface of the individual fibre networks (Fig. 3A). Energy-dispersive X-ray analysis across the aggregates showed iron and oxygen, indicating the metal oxide was distributed homogeneously within the aggregate structure (Fig. 3A). Cross sections of these aggregates shown with TEM further suggest a homogeneous structure (Fig. 5).

Examination of the composite by TEM without negative staining (Fig. 4, SI Fig. S1) showed the iron-C-CNF network was composed of single fibrils having a cross section of 3–4.5 nm or double fibrils in the range of 5.5–8 nm (SI Fig. S1) and as well as strongly scattering elements in the order of 5.5–8 nm, distributed along the lateral dimensions of the network. Under normal circumstances, cellulose-based samples require staining with uranyl acetate or similar heavy metal stains to be visible. However, in the present case, the composite fibre structure was visible due to the presence of iron oxide nanoparticles bound to individual carboxymethyl cellulose fibrils.

Based on the presence of iron oxide in both the aggregates and fibril-like structures within the sample, it would seem feasible that initially the metal salts hydrolyse to form hydrated species, which then coordinate with partially deprotonated C-CNFs. The addition of base leads to further deprotonation of the C-CNFs and production of iron hydroxide species that nucleate to form magnetite at high pH (Seisenbaeva and Kessler, 2014), with the surface remaining iron coordinated to the carboxymethylated cellulose nanofibrils. However, this does not explain the formation of both the “fibre-like” assemblies and larger aggregates. Using electron microscopy and AFM, our investigation revealed three distinct composite structures. This included self-assembled fibril structures containing surface-bound iron oxide nanoparticles, larger C-CNF aggregates with iron oxide nanoparticles in the range of a few nanometers, and large iron oxide particles that formed on the surface of fibril aggregates, the latter stimulated by Ostwald ripening. The larger particles may result from both aggregation and Ostwald ripening, although the larger crystal domain size for the composite indicates domination of the Ostwald ripening phenomenon. It is assumed however, that the source of C-CNFs will play a significant role in the formation of the observed structures. In this study, the C-CNFs were derived from wood and had uniform particle sizes in the range of 3–4.5 nm for single fibrils according to TEM.

To determine whether the iron oxides are precipitated along the outer regions of the large C-CNFs network, or were incorporated within the bulk of the aggregates, samples were embedded, sectioned and

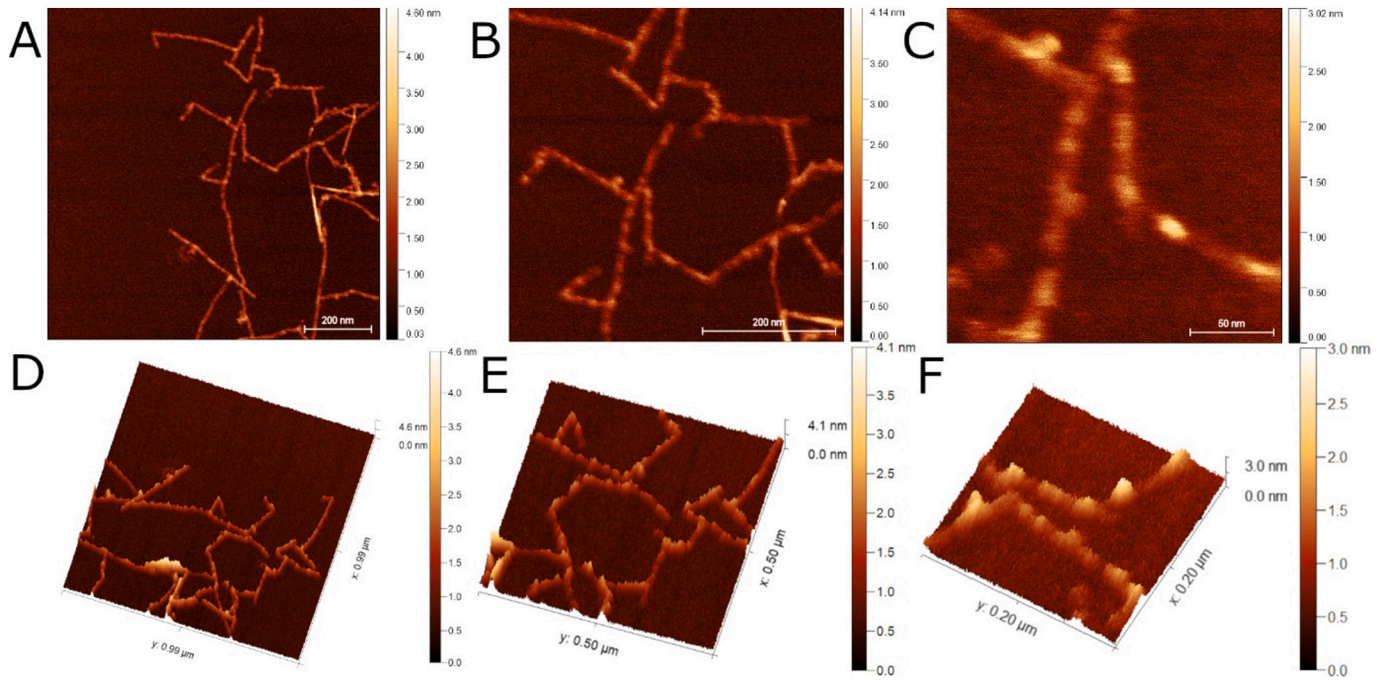

Fig. 2. Scanasyst AFM images of an Iron-oxide carboxymethyl cellulose composite. Top down view at 512 px resolution and A) 1 × 1 µm, B) 500 × 500 nm, C) 200 × 200 nm scan sizes. 3D view a composite at D) 1 × 1 µm, E) 500 × 500 nm and F) 200 × 200 nm.

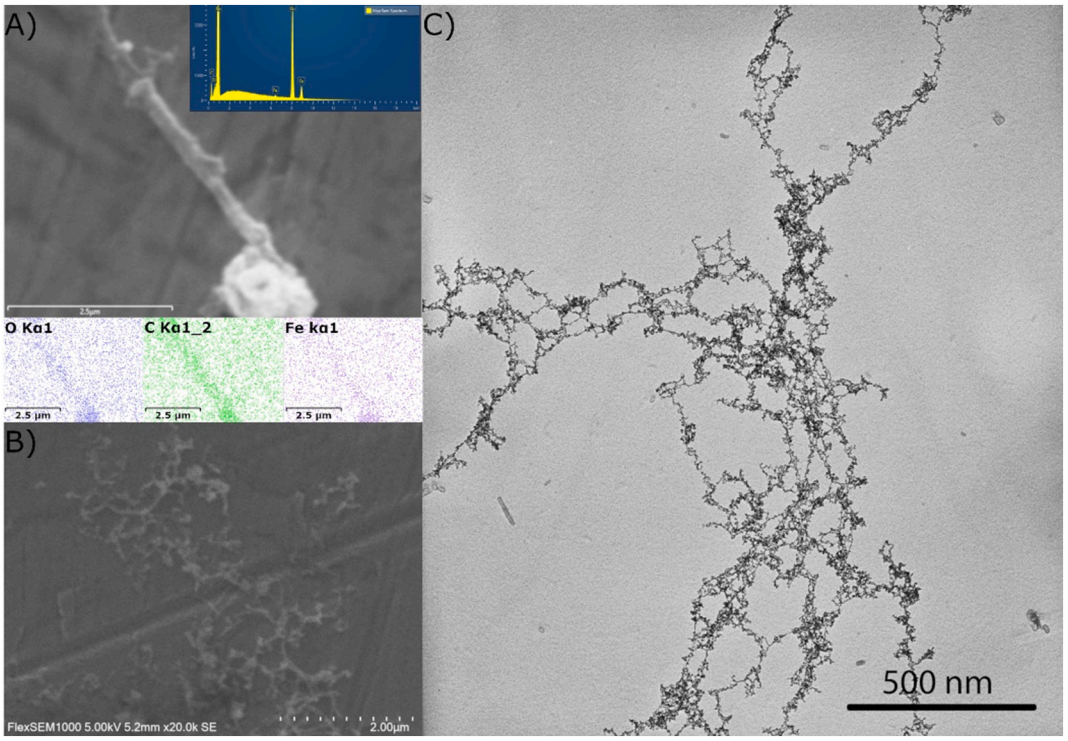

Fig. 3. A) SEM-EDS image of a large aggregate showing the presence and distribution of carbon, oxygen and iron, attributed to carboxymethylated cellulose nanofibrils and iron oxide respectively. B) SEM image of the iron oxide – C-CNF. C) TEM image without staining of iron oxide-C-CNF.

examined by TEM to provide additional information on the ultrastructural nature of the composite material.

As shown in Figs. 3–5 and S1, Fig. S1, the iron oxides were present in three major forms, including, iron oxide aggregates, inclusion of iron oxides within the C-CNF aggregate structure, and adsorption onto the C-CNF fibril surfaces. While the surface adsorbed iron oxide nanoparticles grew into large sizes due to Ostwald ripening (i.e. ca. 5,5–8 nm), the iron oxide nanoparticles encapsulated within the C-CNF structure remained in the order of 1,5–2,5 nm. This observation is in good agreement with calculations of the average size of crystalline domain applying the Scherrer formula. It indicates that carboxymethylated cellulose nanofibrils not only allow for the formation of C-CNF-iron oxide network clusters, it is also effective in retaining the iron oxide particle size range to a few nanometers, so long as the particles are encapsulated by

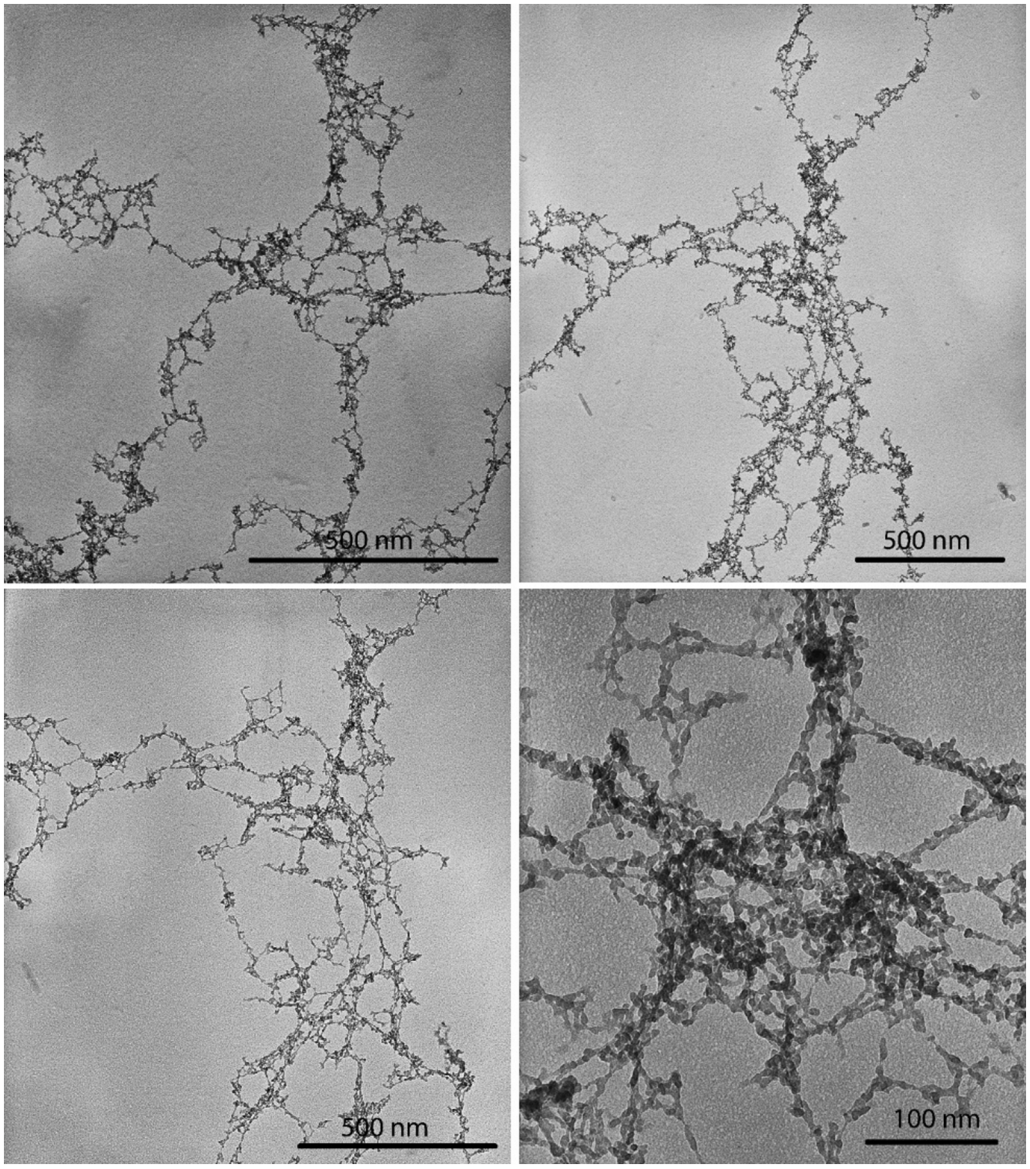

Fig. 4. TEM Images of iron-oxide carboxymethyl cellulose composites without staining and at varying magnification.

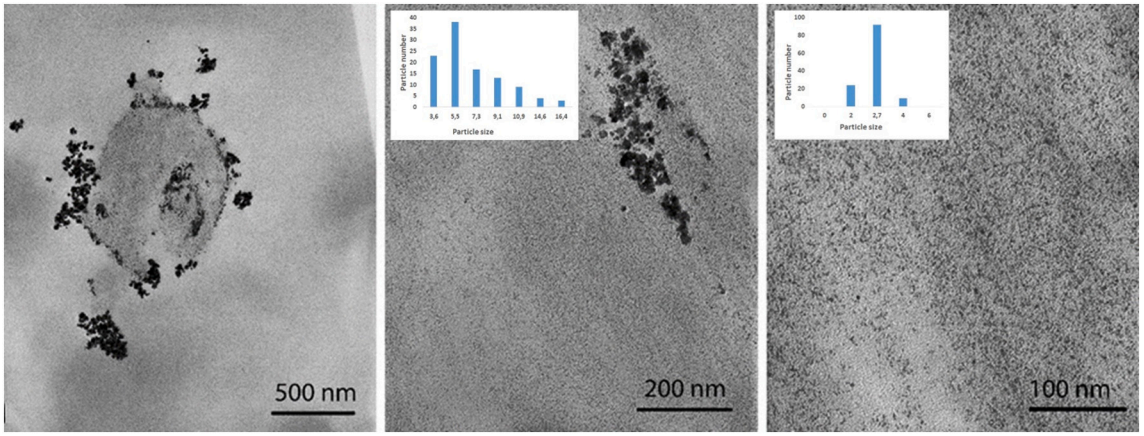

Fig. 5. TEM images of a cross-sectioned resin embedded iron oxide – C-CNFs. Large aggregates are visible on the surface (inset shows the particle size distribution in nm) and open structure of the iron-cellulose composite, while smaller particles appear aligned with individual fibrils (inset shows the particle size distribution in nm).

cellulose fibrils and not present on the surface where Ostwald ripening can occur. Ostwald ripening otherwise sometimes called isothermal distillation is a phenomenon associated with minimization of the surface energy in a precipitate, which results in dissolution of smaller particles and simultaneous growth of the larger ones in the system (Voorhees, 1985). Whether the formation of these large composite aggregates is caused by the formation of small iron oxide particles after bonding of ionic iron to C-CNF or by the intercalation of the iron oxide particles within the C-CNF after metal oxide formation remains unknown. TEM suggests the iron oxides associate with the outer regions of the nano-sized C-CNFs, following the orientation of the individual cellulose fibrils (Figs. 5, S, S1). The statistic distribution of sizes for single-domain particles according to TEM (see Fig. 5) shows that it is clearly smaller inside the fibres 2.0–4.0 nm compared to that on their surface 3.6–16.4 nm, indicating that it was in the first hand Ostwald ripening that produced the larger particles on the surface.

3.4. Drug adsorption and desorption

Fe_3O_4 NPs are of interest not only for their magnetic properties but also for their optical properties, as they are known to display photothermal conversion which may be exploited for therapy and drug delivery (Estelrich & Busquets, 2018; Johnson et al., 2018; Sadat et al., 2014; Wang et al., 2014). In order to examine the potential of the composite material as a drug delivery vehicle, we tested the adsorption and desorption of tetracycline, a broad-spectrum antibiotic. After 72 hour contact time, tetracycline showed a maximum drug adsorption of 62 μg/mg (79%) at room temperature with up to 27 μg/mg (35%) within the first 240 min indicating that the initial adsorption is fast and thereafter slows down (Fig. 6A).

To test the viability of the composite for drug delivery and the influence daylight plays on the release of tetracycline, samples were prepared in batches and split equally. One part was exposed to a daylight lamp during desorption, and the other kept dark by wrapping in foil. Citrate buffer was added and release of tetracycline followed by UV–VIS (Fig. 6B). Initial drug release was relatively slow with an approximate 11% release in the absence of light and 20% release in light after 3 h. This increases to 33 and 85% with- and without light respectively, after 2 days indicating that the release desorption rate of tetracycline was strongly influenced by daylight.

4. Conclusions

In this work, we demonstrated the synthesis of a magnetically responsive composite material based on carboxymethyl cellulose and in-situ synthesized magnetite, that self-assembled into fibre-like nanostructures which were characterized by AFM, SEM, TEM, FTIR, TGA and PXRD. The material displayed stable magnetic characteristics on storage, both in solid state and in solution. In addition, the novel material was studied in solution state as a potential drug vehicle for the delivery of tetracycline. Thus, the main hypothesis of this work was proved valid.

Carboxymethylated cellulose nanofibrils derived from wood were successfully decorated with iron oxide particles in an in situ process so that magnetic iron oxide particles were of relative uniform size and assembled into larger composite structures together with cellulose. These structures could be divided into three broad categories: i) Large C-CNF aggregates where the iron oxide nanoparticle size was small with growth limited by the C-CNF structure; ii) large iron oxide particles that form on the surface of the fibre aggregates, where particle growth is stimulated by Ostwald ripening, and iii) cellulose-iron oxides forming long fibre networks comprising iron oxide and cellulose with longitudinal dimensions far exceeding that of the initial components. For the fibre-like networks, it is highly likely that the morphology and pH response of both the metal oxide and C-CNF play a crucial role in its formation. Variations in cellulose source and synthetic conditions may have significant influence on the overall structures formed. The phase of iron oxide synthesized in this method is the magnetically responsive magnetite, which will oxidize to iron(II)-deficient maghemite with time in the presence of oxygen. This method is simple and cost-effective, which can lead to the development of further magnetically relevant materials. However, the synthesis of the “fibre-like” structures remains difficult with subtle changes in synthetic conditions having a profound effect on the structures obtained.

Electronic supporting information includes additional details on TEM, XRD and TGA studies, and demonstration of magnetic properties of obtained materials (as photo and video evidence). Supplementary data to this article can be found online at https://doi.org/10.1016/j.carbpol.2022.119560.

CRediT authorship contribution statement

TB has performed all the synthetic work and adsorption and desorption experiments and wrote the draft of the manuscript, GD has performed the TEM characterization and contributed to formulation and

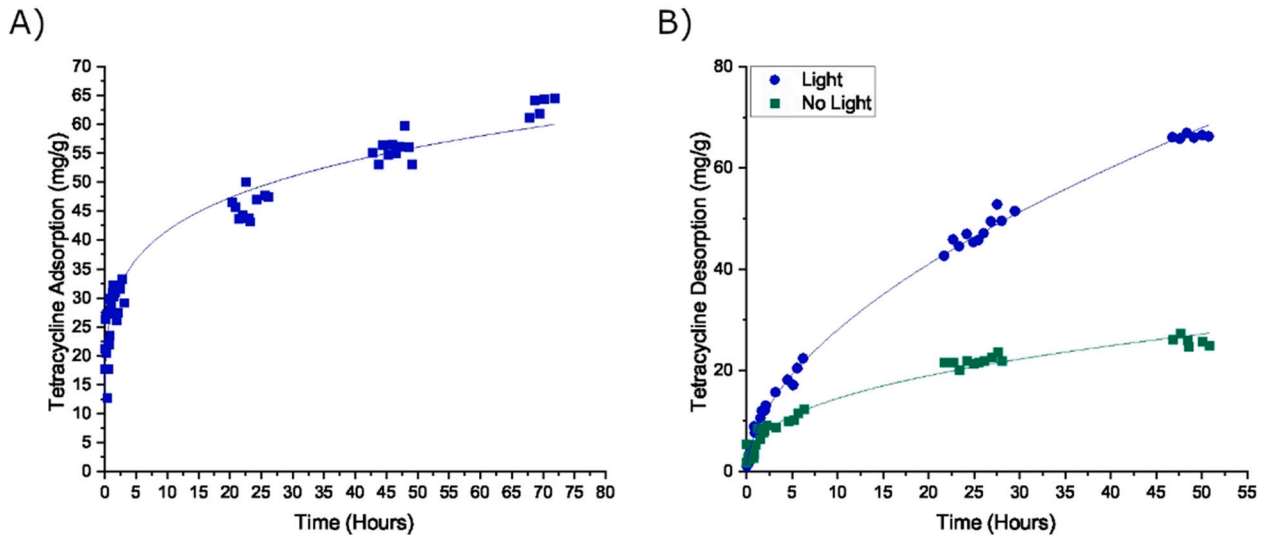

Fig. 6. Tetracycline adsorption and desorption. A) Tetracycline adsorption in mg/g and B) tetracycline desorption in mg/g as a function of time.

language editing of the manuscript, DH and PS have performed the magnetic measurements and helped with their interpretation, VK contributed with XRD measurements, HG and KH provided the C-CNF material and helped with interpretation of data, GS contributed with the project idea, TGA, FTIR, AFM and ESEM measurements and performed the final editing of the manuscript. All authors participated actively in discussion of results and contributed to editing of the manuscript.

Declaration of competing interest

The authors declare that they have no affiliations with or involvement in any organization or entity with any financial interest or non-financial interest in the subject matter or material discussed in this manuscript.

Acknowledgements

The authors are grateful to Professor Sidney Ribeiro for valuable discussions.

Funding

The authors express their gratitude to the Swedish Research Council STINT for support of the grant Nanocellulose Based Materials for Environmental and Theranostic Applications and to the Faculty of Natural Resources and Agricultural Sciences, SLU for support of TB PhD position.

References

Aaen, R., Simon, S., Wernersson Brodin, F., & Syverud, K. (2019). The potential of TEMPO-oxidized cellulose nanofibrils as rheology modifiers in food systems. *Cellulose, 26*, 5483–5496.

Abbasi Pour, S., Shaterian, H. R., Afradi, M., & Yazdani-Elah-Abadi, A. (2017). Carboxymethyl cellulose (CMC)-loaded co-cu doped manganese ferrite nanorods as a new dual-modal simultaneous contrast agent for magnetic resonance imaging and nanocarrier for drug delivery system. *Journal of Magnetism and Magnetic Materials, 438*, 85–94. https://doi.org/10.1016/j.jmmm.2017.04.069

Arantes, A. C. C., Dauzacker, L. C. L., Bianchi, M. L., Wood, D. F., Williams, T. G., Orts, W. J., … Almeida, C.d. G. (2017). Renewable hybrid nanocatalyst from magnetite and cellulose for treatment of textile effluents. *Carbohydrate Polymers, 163*, 101–107. https://doi.org/10.1016/j.carbpol.2017.01.007

Biliuta, G., Sacarescu, L., Socoliuc, V., Iacob, M., Gheorghe, L., Negru, D., & Coseri, S. (2017). Carboxylated polysaccharides decorated with ultrasmall magnetic nanoparticles with antibacterial and MRI properties. *Macromolecular Chemistry and Physics, 218*(10), 1700062. https://doi.org/10.1002/macp.201700062

Chaabane, L., Chahdoura, H., Mehdaoui, R., Snoussi, M., Beyou, E., Lahcini, M., & Baouab, M. H. V. (2020). Functionalization of developed bacterial cellulose with magnetite nanoparticles for nanobiotechnology and nanomedicine applications. *Carbohydrate Polymers, 247*, Article 116707. https://doi.org/10.1016/j.carbpol.2020.116707

Chen, X., Ye, Z., Yang, F., Feng, J., Li, Z., Huang, C., Ke, Q., & Yin, Y. (2020). Magnetic cellulose microcrystals with tunable magneto-optical responses. *Applied Materials Today, 20*, Article 100749. https://doi.org/10.1016/j.apmt.2020.100749

Dimic-Misic, K., Gane, P. A. C., & Paltakari, J. (2013). Micro- and nanofibrillated cellulose as a rheology modifier additive in CMC-containing pigment-coating formulations. *Industrial & Engineering Chemistry Research, 52*(45), 16066–16083. https://doi.org/10.1021/ie4028878

Dimic-Misic, K., Phiri, J., Nieminen, K., Maloney, T., & Gane, P. (2019). Characterising exfoliated few-layer graphene interactions in co-processed nanofibrillated cellulose suspension via water retention and dispersion rheology. *Materials Science and Engineering: B, 242*, 37–51. https://doi.org/10.1016/j.mseb.2019.03.001

Ellid, M. S., Murayed, Y. S., Zoto, M. S., Musić, S., & Popović, S. (2003). Chemical reduction of hematite with starch. *Journal of Radioanalytical and Nuclear Chemistry, 258*(2), 299–305. https://doi.org/10.1023/A:1026285721065

Estelrich, J., & Busquets, M. A. (2018). Iron oxide nanoparticles in photothermal therapy. *Molecules, 23*(7), 1567. https://doi.org/10.3390/molecules23071567

Favier, V., Chanzy, H., & Cavaille, J. Y. (1995). Polymer nanocomposites reinforced by cellulose whiskers. *Macromolecules, 28*(18), 6365–6367. https://doi.org/10.1021/ma00122a053

Galland, S., Andersson, R. L., Salajková, M., Ström, V., Olsson, R. T., & Berglund, L. A. (2013). Cellulose nanofibers decorated with magnetic nanoparticles – synthesis, structure and use in magnetized high toughness membranes for a prototype loudspeaker. *Journal of Materials Chemistry C, 1*(47), 7963–7972. https://doi.org/10.1039/C3TC31748J

Grunert, M., & Winter, W. T. (2002). Nanocomposites of cellulose acetate butyrate reinforced with cellulose nanocrystals. *Journal of Polymers and the Environment, 10*(1), 27–30. https://doi.org/10.1023/A:1021065905986

Hao, J., Zhang, W., Wang, H., Ziya, N., Luo, Y., Jia, P., Zhang, G., & Ng, T. (2021). Purification and properties of a laccase from the mushroom Agaricus sinodeliciosus. *Biotechnology and Applied Biochemistry, 68*(2), 297–306. https://doi.org/10.1002/bab.1926

Hartings, M., Douglass, K. O., Neice, C., & Ahmed, Z. (2018). Humidity responsive photonic sensor based on a carboxymethyl cellulose mechanical actuator. *Sensors and Actuators B: Chemical, 265*, 335–338. https://doi.org/10.1016/j.snb.2018.03.065

He, X., Lu, W., Sun, C., Khalesi, H., Mata, A., Andaleeb, R., & Fang, Y. (2021). Cellulose and cellulose derivatives: Different colloidal states and food-related applications. *Carbohydrate Polymers, 255*, Article 117334. https://doi.org/10.1016/j.carbpol.2020.117334

Hon, D. N.-S. (1994). Cellulose: A random walk along its historical path. *Cellulose, 1*(1), 1–25. https://doi.org/10.1007/BF00818796

Hu, L., Choi, J. W., Yang, Y., Jeong, S., Mantia, F. L., Cui, L.-F., & Cui, Y. (2009). Highly conductive paper for energy-storage devices. *Proceedings of the National Academy of Sciences, 106*(51), 21490–21494. https://doi.org/10.1073/pnas.0908858106

Ishii, M., Nakahira, M., & Yamanaka, T. (1972). Infrared absorption spectra and cation distributions in (Mn, Fe)3O4. *Solid State Communications, 11*(1), 209–212. https://doi.org/10.1016/0038-1098(72)91162-3

Johnson, R. J. G., Schultz, J. D., & Lear, B. J. (2018). Photothermal effectiveness of magnetite nanoparticles: Dependence upon particle size probed by experiment and simulation. *Molecules, 23*(5), 1234. https://doi.org/10.3390/molecules23051234

Khalilzadeh, M. A., Tajik, S., Beitollahi, H., & Venditti, R. A. (2020). Green synthesis of magnetic nanocomposite with iron oxide deposited on cellulose nanocrystals with copper (Fe3O4@CNC/Cu): Investigation of catalytic activity for the development of a venlafaxine electrochemical sensor. *Industrial & Engineering Chemistry Research, 59*(10), 4219–4228. https://doi.org/10.1021/acs.iecr.9b06214

Kim, J., Yun, S., & Ounaies, Z. (2006). Discovery of cellulose as a smart material. *Macromolecules, 39*(12), 4202–4206. https://doi.org/10.1021/ma060261e

Klemm, D., Heublein, B., Fink, H.-P., & Bohn, A. (2005). Cellulose: Fascinating biopolymer and sustainable raw material. *Angewandte Chemie International Edition, 44*(22), 3358–3393. https://doi.org/10.1002/anie.200460587

Klotz, M., Ayral, A., Guizard, C., Ménager, C., & Cabuil, V. (1999). Silica coating on colloidal maghemite particles. *Journal of Colloid and Interface Science, 220*(2), 357–361. https://doi.org/10.1006/jcis.1999.6517

Li, Y., Zhu, H., Gu, H., Dai, H., Fang, Z., Weadock, N. J., Guo, Z., & Hu, L. (2013). Strong transparent magnetic nanopaper prepared by immobilization of Fe3O4 nanoparticles in a nanofibrillated cellulose network. *Journal of Materials Chemistry A, 1*(48), 15278–15283. https://doi.org/10.1039/C3TA12591B

Lim, W., Douglas, E. A., Kim, S.-H., Norton, D. P., Pearton, S. J., Ren, F., Shen, H., & Chang, W. H. (2009). High mobility InGaZnO4 thin-film transistors on paper. *Applied Physics Letters, 94*(7), Article 072103. https://doi.org/10.1063/1.3086394

Musić, S., Šarić, A., Popović, S., Nomura, K., & Sawada, T. (2000). Forced hydrolysis of Fe3+ ions in NH4Fe(SO4)2 solutions containing urotropin. *Croatica Chemica Acta, 73*(2), 541–567.

Oun, A. A., & Rhim, J.-W. (2017). Characterization of carboxymethyl cellulose-based nanocomposite films reinforced with oxidized nanocellulose isolated using ammonium persulfate method. *Carbohydrate Polymers, 174*, 484–492. https://doi.org/10.1016/j.carbpol.2017.06.121

Sacui, I. A., Nieuwendaal, R. C., Burnett, D. J., Jorfi, M., Weder, C., Foster, E. J., Olsson, R. T., Gilman, J. W., & Stranick, S. J. (2014). Comparison of the properties of cellulose nanocrystals and cellulose nanofibrils isolated from bacteria, tunicate, and wood processed using acid, enzymatic, mechanical, and oxidative methods. *ACS Appl. Mater. Interfaces, 6*, 6127–6138. https://doi.org/10.1021/am500359f

Sadat, M. E., Kaveh Baghbador, M., Dunn, A. W., Wagner, H. P., Ewing, R. C., Zhang, J., Xu, H., Pauletti, G. M., Mast, D. B., & Shi, D. (2014). Photoluminescence and photothermal effect of Fe3O4 nanoparticles for medical imaging and therapy. *Applied Physics Letters, 105*(9), Article 091903. https://doi.org/10.1063/1.4895133

Seisenbaeva, G. A., & Kessler, V. G. (2014). Precursor directed synthesis – "molecular" mechanisms in the soft chemistry approaches and their use for template-free synthesis of metal, metal oxide and metal chalcogenide nanoparticles and nanostructures. *Nanoscale, 6*, 6229–6244. https://doi.org/10.1039/C3NR06336D

Souza, S. F., Mariano, M., De Farias, M. A., & Bernardes, J. S. (2019). Effect of depletion forces on the morphological structure of carboxymethyl cellulose and micro/nano cellulose fiber suspensions. *Journal of Colloid and Interface Science, 538*, 228–236. https://doi.org/10.1016/j.jcis.2018.11.096

Thanh, N. T. H. (Ed.). (2012). *Magnetic Nanoparticles: From Fabrication to Clinical Applications* (1st ed.). CRC Press. ISBN-10: 1439869324.

Transforming our world: The 2030 Agenda for Sustainable Development, n.d. Transforming our world: The 2030 agenda for sustainable development | Department of Economic and Social Affairs. (n.d.). Retrieved November 22, 2021, from https://sdgs.un.org/2030agenda.

Voorhees, P. W. (1985). The theory of ostwald ripening. *Journal of Statistical Physics, 38*, 231–252.

Wågberg, L., Decher, G., Norgren, M., Lindström, T., Ankerfors, M., & Axnäs, K. (2008). The build-up of polyelectrolyte multilayers of microfibrillated cellulose and cationic polyelectrolytes. *Langmuir, 24*(3), 784–795. https://doi.org/10.1021/la702481v

Wang, H., Shen, J., Li, Y., Wei, Z., Cao, G., Gai, Z., Hong, K., Banerjee, P., & Zhou, S. (2014). Magnetic iron oxide–fluorescent carbon dots integrated nanoparticles for dual-modal imaging, near-infrared light-responsive drug carrier and photothermal therapy. *Biomaterials Science, 2*(6), 915–923. https://doi.org/10.1039/C3BM60297D

Wu, H., Teng, C., Tian, H., Li, Y., & Wang, J. (2018). Fabrication of functional magnetic cellulose nanocomposite membranes for controlled adsorption of protein. *Cellulose, 25*(5), 2977–2986. https://doi.org/10.1007/s10570-018-1750-2

Yu, X., Kang, D., Hu, Y., Tong, S., Ge, M., Cao, C., & Song, W. (2014). One-pot synthesis of porous magnetic cellulose beads for the removal of metal ions. *RSC Advances, 4* (59), 31362–31369. https://doi.org/10.1039/C4RA05601A

Yu, X., Tong, S., Ge, M., Zuo, J., Cao, C., & Song, W. (2012). One-step synthesis of magnetic composites of cellulose@iron oxide nanoparticles for arsenic removal. *Journal of Materials Chemistry A, 1*(3), 959–965. https://doi.org/10.1039/C2TA00315E